Digital Analytics and Robotics for Sustainable Forestry

CL4-2021-DIGITAL-EMERGING-01
Grant agreement no: 101070405

DELIVERABLE 2.3

Active chassis balancing of SAHA robot

Due date: month 24 (August 2024)
Deliverable type: R
Lead beneficiary: ETH Zurich

Dissemination Level: PUBLIC

Main author: Fang Nan, Pol Eyschen, Fan Yang, Marco Hutter

Contents

1 Introduction

The SAHA robot, as shown in Fig. 1, is a (semi-)autonomous forest logging machine developed in the DigiForest project [1]. The design is based on RCM Harveri, a small, radio-controlled harvester intended mainly for first thinning and energy wood harvesting for trees up to 30 cm diameter.

Figure 1: Picture of a SAHA robot.

As a small-scale forest machine, SAHA has a compact design and a short wheelbase. These characteristics enable SAHA to navigate through dense forests and operate in confined spaces for thinning operations. However, the short wheelbase of SAHA also renders it less stable on uneven terrains, increasing the risk of tipping over and losing rough terrain motility. To address this issue, actuated chassis is commonly used by small-scale forest machines to improve stability. On the SAHA platform, each wheel is installed on a leg that can rotate around a Hip flexion/extension (HFE) joint, as shown in Fig. 2. Each leg is individually actuated by a hydraulic cylinder and can be used to adjust the height of the wheel.

Traditionally, the control of the active chassis is achieved by the operator manually adjusting the height of each wheel to keep all wheels in contact with the ground. To achieve full autonomy, an active chassis balancing control system has been implemented on SAHA. Utilizing the sensors on the robot that has been integrated in the first phase of the project, the balancing control system ensures stable support of the robot in rough terrains and facilitates autonomous tree manipulations in the future. This report presents the active chassis balancing control system of the SAHA robot.

2 Methodology

For an active chassis balancing system, the primary objective is to manage the stability and adaptability of SAHA robots in uneven terrains by automatically adjusting the chassis pose through force regulation. The overall approach is thus composed of two

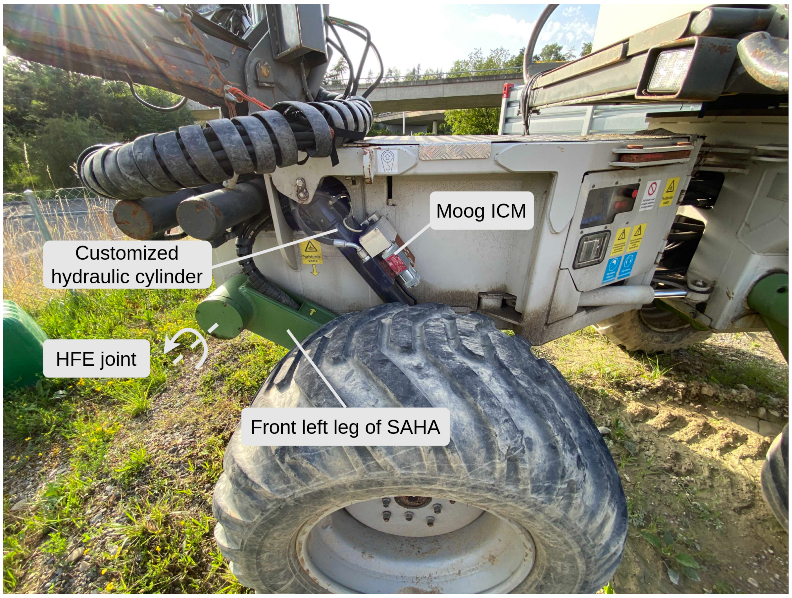

Figure 2: Picture of SAHA's left front wheel. The wheel is mounted on a leg that can rotate around the HFE joint when actuating the hydraulic cylinder.

aspects: the precise force control of hydraulic cylinders on SAHA's HFE joints, and the optimal ground contact force distribution between the four legs.

2.1 Hydraulic Cylinders Force Control

The primary objective of cylinder force control is to regulate the exerted force the hydraulic cylinders without the use of external force sensors such as load cells. We present two approaches for force control: one using high-performance integrated control modules (ICMs) and another using simplified hardware with standard proportional valves and off-the-shelf pressure sensors. For the high performance control, we estimated the cylinder force using the pressure readings from sensors integrated in the hydraulic chambers, accounting for piston velocity and friction forces. This approach provides accurate, high-bandwidth force control, while the solution with simplified hardware excels in scalability and cost-effectiveness.

Friction Modeling While the pressure difference in the hydraulic chambers creates a force on the piston, the actual force exerted by the cylinder is influenced by frictional effects within the system. Therefore, a crucial aspect of the force control strategy is the accurate modeling of friction within the hydraulic system. Based on experience of modeling similar actuators [2], a simple Stribeck model is used to characterize the friction in SAHA HFE cylinders. This model has been extensively verified on calibrated testbenches, and demonstrated high-accuracy force estimation with minimal deviation (less than 1% of maximum force) from actual forces [3].

Integrated Control Module To achieve fast and accurate force control, the low-level force control loop is operated at a high frequency of 10 kHz directly on the ICM module. Each ICM combines a high-performance Moog servo valve with integrated electronics and a microprocessor running the force controller calibrated for the specific cylinder and valve. They are directly mounted on the cylinders to minimize delays and improve performance by not having any hose in between.

Force Control with Simplified Hardware As introduced in D2.2 on hardware integration, the simplified setup only requires additional integration of pressure sensors for force feedback. The force control is implemented without friction modeling and compensation, which is still feasible since the friction in the hydraulic cylinders is relatively low compared to the exerted forces [3]. However, the less-precise valve, hoses to the cylinders, and the disturbance from the friction reduces the performance of the force control loop. A significant delay of up to 200 ms has been observed in the force tracking. Nevertheless, the system is still able to approximately track the desired forces with delay. Since the SAHA robot drives at a relatively low speed, the compromised controller was still tested in the chassis balancing task.

2.2 Chassis Balancing Control

The chassis balancing controller is designed to optimally distribute contact forces based on the robot's state, including the configuration of its legs and the position and orientation of the vehicle body. We use a quasi-static approximation and small-angle assumption to simplify the dynamics of the harvester, and use Virtual Model Control (VMC) to regulate the pose of SAHA body.

Model Simplification The rigid body dynamics of SAHA can be described by the equation of motion of floating-base systems

$$\mathbf{M}\ddot{\mathbf{q}} + \mathbf{b} + \mathbf{g} + \boldsymbol{\lambda}_c = \mathbf{S}^T\boldsymbol{\tau} + \boldsymbol{\lambda}^{\text{dist}} \tag{1}$$

with the mass matrix $\mathbf{M}$, the Coriolis and centrifugal vector $\mathbf{b}$, the gravitational vector $\mathbf{g}$, the projected contact forces $\boldsymbol{\lambda}_c$, the actuator torques $\boldsymbol{\tau}$, and the projected disturbance forces $\boldsymbol{\lambda}^{\text{dist}}$.

Given the slow motion of the excavator, a quasi-static assumption can be applied, which simplifies the dynamic model by neglecting acceleration and Coriolis forces. Thus the equation of motion can be simplified to

$$\sum_{i=1}^{n_c} \mathbf{J}_{C_i}^T \mathbf{F}_{C_i} - \sum_{i=1}^{n} \mathbf{J}_{S_i}^T \mathbf{F}_{g_i} = \mathbf{S}^T\boldsymbol{\tau} + \boldsymbol{\lambda}^{\text{dist}}, \tag{2}$$

where $\mathbf{J}_{C_i}$ are the contact Jacobians of contact points i, $\mathbf{F}_{C_i}$ the contact forces, $\mathbf{J}_{S_i}$ the Jacobians evaluated at the COG of link i, and $\mathbf{F}_{g_i}$ the gravitational forces on link i.

The generalized disturbance forces $\boldsymbol{\lambda}^{\text{dist}}$ encodes change in external load mostly due to the different configurations of the arm and the payload, and it is assumed to be acting on the base (chassis) of the harvester. Thus we could separate (2) into base Degrees of Freedoms (DoFs) and leg DoFs. As vehicle body will mostly stay in a horizontal position with only small deviations, we can further simplify the model by assuming that the contact forces are mostly vertical and only consider the z, roll, and pitch DoFs of the base. Finally, the equation of motion can be reduced to

$$\sum_{i=1}^{n_c} F_{(Cz)_i} - \sum_{i=1}^{n} m_i g = \lambda_z^{\text{dist}} \tag{3}$$

$$\sum_{i=1}^{n_c} \begin{pmatrix} y_{BC_i} \\ -x_{BC_i} \end{pmatrix} F_{(Cz)_i} - \sum_{i=1}^{n} \begin{pmatrix} y_{BS_i} \\ -x_{BS_i} \end{pmatrix} m_i g = \lambda_{(roll,pit)}^{\text{dist}} \tag{4}$$

$$\sum_{i=1}^{n_c} \mathbf{j}_{(Ci,z)_i}^T F_{(Cz)_i} - \sum_{i=1}^{n} \mathbf{j}_{(Si,z)_i}^T m_i g = \boldsymbol{\tau}, \tag{5}$$

where y_{BC_i} and x_{BC_i} are the y and x coordinates of the contact points i in the base frame, and y_{BS_i} and x_{BS_i} are the coordinates of the COG of link i in the base frame. $\mathbf{j}_{(Ci,z)_i}$ and $\mathbf{j}_{(Si,z)_i}$ are the z-direction components of the contact and COG Jacobians $\mathbf{J}_{C_i}$ and $\mathbf{J}_{S_i}$.

The resulting model focuses on maintaining force and torque equilibrium, allowing the system to be controlled as a static structure, primarily influenced by the weight distribution and external forces.

Virtual Model Control We apply the classical VMC [4] to generate virtual forces and moments that drive the harvester towards a desired configuration. The desired virtual forces applied to the chassis of the harvester is calculated based on the desired height and orientation of the chassis with a PID controller.

$$\begin{aligned} F_v &= \text{PID}^p \left(z^{\text{des}} - z_b \right) \\ T_v &= \text{PID}^r \left(\varphi^{\text{des}} - \varphi \right) \end{aligned} \tag{6}$$

Contact Force Optimization The desired virtual forces and moments on the chassis have to be created by the contact forces on the legs. Combining the base dynamic part of the equation of motion (3) and (4) with the desired virtual forces and moments, we can establish the following relationship between the contact forces and the virtual forces and moments.

$$\begin{bmatrix} 1 & \dots & 1 \\ y_{BC_1} & \dots & y_{BC_4} \\ -x_{BC_1} & \dots & -x_{BC_4} \end{bmatrix} \begin{pmatrix} F_{(Cz)_1} \\ F_{(Cz)_2} \\ F_{(Cz)_3} \\ F_{(Cz)_4} \end{pmatrix} = \sum_{i=1}^{n} m_i g \begin{pmatrix} 1 \\ y_{BS_i} \\ -x_{BS_i} \end{pmatrix} + \begin{pmatrix} BF_v \\ B\mathbf{T}_v \end{pmatrix} + \begin{pmatrix} m_{\text{arm}} g \\ 0 \\ 0 \end{pmatrix} \tag{7}$$

As we have four contact forces and only three equations, we formulate the force distribution problem as a quadratic optimization problem, where the goal is to find the minimal ground reaction forces that satisfy (7) and adhering to constraints on force magnitudes. Since (7) is a linear equation on the contact force vector in the form $\mathbf{AF} = \mathbf{b}$, we can formulate the optimization problem as

$$\begin{aligned} \underset{\mathbf{F}}{\text{minimize}} \quad & \mathbf{F}^T\mathbf{F} \\ s.t. \quad & \mathbf{AF} = \mathbf{b} \\ & \mathbf{F}_{\text{min}} \leq \mathbf{F} \leq \mathbf{F}_{\text{max}}. \end{aligned} \tag{8}$$

The solution to (8) provides the optimal distribution of contact forces, and can be substituted into (5) to calculate the required actuator torques on the corresponding HFE joints.

3 Experiments

Figure 3: Experiment of SAHA driving over logs.

We evaluated the implemented controller in a variety of environments, from artificial obstacles on flat ground to real forest terrain. Compared to the larger machines with chassis balancing [2], the SAHA robot has a smaller HFE range of motion. This limits the adjustability of SAHA's chassis attitude, particularly in the pitch direction due to the longer distance between the front and rear wheels. It is therefore not always possible to maintain a horizontal pitch when the terrain gets complicated. As a compromise, we define the reference pitch angle to be halfway between the horizontal direction and being parallel to the slope of the terrain, under the constraint that all wheels maintain contact with the ground. In the roll direction, we have better adjustability as the narrow machine has a small distance between the left and right

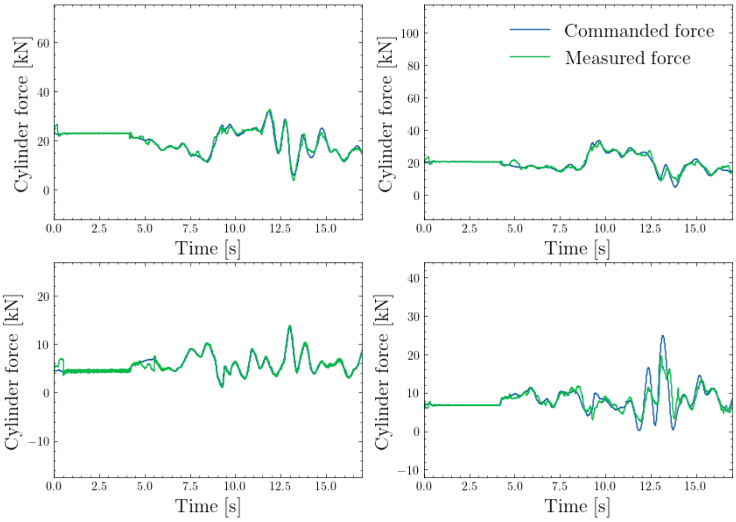

Figure 4: Reference and measured commands on the four leg support joints of SAHA during a driving experiment on uneven terrain. Each subplot corresponds to one leg of the robot.

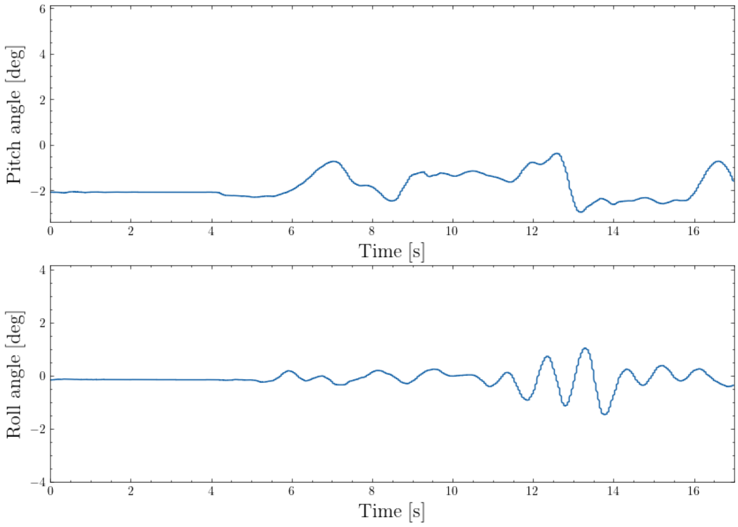

Figure 5: Measured pitch (top) and roll (bottom) during the same driving experiment on SAHA.

wheels. The reference roll angle is thus kept horizontal.

Fig. 3 shows an experiment in which SAHA drives over two logs artificially placed on a test field. Plots of the commanded and measured joint efforts, and the measured pitch and roll of the machine, are shown in Fig. 4 and Fig. 5, respectively. It can be observed that the cylinder controllers are able to track the reference forces well, and the machine maintains a stable orientation during the experiment with both pitch and roll angle deviations kept within a few degrees.

Similar experiment is also performed on another SAHA robot, which uses the simplified hardware setup. Despite the lower force control bandwidth, the machine is also able to maintain all wheels in contact with the ground during a driving experiment on uneven terrain, as shown in Fig. 6.

Figure 6: SAHA-2 with active chassis control driving over a tree trunk with its right wheels. The active chassis balancing ensures contact of each wheel during the process.

4 Summary

This report presents the active chassis balancing control system of the SAHA robot, including the single cylinder force control and the virtual model control for balancing the chassis. The algorithm has successfully achieved the goal of chassis stabilization on the SAHA platform. We also tested the algorithm on a SAHA robot without the expensive ICM modules, and stable ground contact for all wheels was still achieved.

In the future, we plan to continue testing the controller in extensive autonomous and teleoperated field trials, and further improve the performance of the controller.

References

[1] E. Jelavic, T. Kapgen, S. Kerscher, D. Jud, and M. Hutter, “Harveri : A Small (Semi-)Autonomous Precision Tree Harvester,” in *Innovation in Forestry Robotics: Research and Industry Adoption, ICRA 2022 IFRRIA Workshop*, 2022.

[2] D. Jud, S. Kerscher, M. Wermelinger, E. Jelavic, P. Egli, P. Leemann, G. Hottiger, and M. Hutter, “HEAP - The autonomous walking excavator,” *Automation in Construction*, vol. 129, p. 103783, Sept. 2021.

[3] M. Hutter, P. Leemann, G. Hottiger, R. Figi, S. Tagmann, G. Rey, and G. Small, “Force Control for Active Chassis Balancing,” *IEEE/ASME Transactions on Mechatronics*, vol. 22, pp. 613–622, Apr. 2017. Conference Name: IEEE/ASME Transactions on Mechatronics.

[4] J. Pratt, C.-M. Chew, A. Torres, P. Dilworth, and G. Pratt, “Virtual model control: An intuitive approach for bipedal locomotion,” *The International Journal of Robotics Research*, vol. 20, no. 2, pp. 129–143, 2001.